MIT Libraries | DSpace@MIT

MIT Open Access Articles

Coarsening by network restructuring in model nanoporous gold

The MIT Faculty has made this article openly available. ***Please share*** how this access benefits you. Your story matters.

Citation: Kolluri, Kedarnath, and Michael J. Demkowicz. "Coarsening by Network Restructuring in Model Nanoporous Gold." Acta Materialia 59, no. 20 (December 2011): 7645–7653.

As Published: http://dx.doi.org/10.1016/j.actamat.2011.08.037

Persistent URL: http://hdl.handle.net/1721.1/101910

Version: Original manuscript: author's manuscript prior to formal peer review

Terms of use: Creative Commons Attribution-NonCommercial-NoDerivs License

Massachusetts Institute of Technology

Elsevier Editorial System(tm) for Acta Materialia
Manuscript Draft

Manuscript Number: A-11-530R1

Title: Coarsening by Network Restructuring in Model Nanoporous Gold

Article Type: Full Length Article

Keywords: coarsening, foams, nanoporous metals, modeling

Corresponding Author: Mr Kedarnath Kolluri,

Corresponding Author's Institution: Massachusetts Institute of Technology

First Author: Kedarnath Kolluri, Ph.D.

Order of Authors: Kedarnath Kolluri, Ph.D.; Michael Demkowicz, Ph.D.

Abstract: Using atomistic modeling, we show that restructuring of the network of interconnected ligaments causes coarsening in a model of nanoporous gold. The restructuring arises from the collapse of some ligaments onto neighboring ones and is enabled by localized plasticity at ligaments and nodes. This mechanism may explain the occurrence of enclosed voids and reduction in volume in nanoporous metals during their synthesis. An expression is developed for the critical ligament radius below which coarsening by network restructuring may occur spontaneously, setting a lower limit to the ligament dimensions of nanofoams.

*Text only
Click here to view linked References

Coarsening by Network Restructuring in Model Nanoporous Gold

Kedarnath Kolluri[a,*], Michael J. Demkowicz[a]

[a] *Department of Materials Science and Engineering, Massachusetts Institute of Technology, Cambridge, MA 02139*

Abstract

Using atomistic modeling, we show that restructuring of the network of interconnected ligaments causes coarsening in a model of nanoporous gold. The restructuring arises from the collapse of some ligaments onto neighboring ones and is enabled by localized plasticity at ligaments and nodes. This mechanism may explain the occurrence of enclosed voids and reduction in volume in nanoporous metals during their synthesis. An expression is developed for the critical ligament radius below which coarsening by network restructuring may occur spontaneously, setting a lower limit to the ligament dimensions of nanofoams.

1. Introduction

Nanoporous metals are sponge-like metallic structures with open-cell network structure. They are comprised of interconnected ligaments of nanometer-scale characteristic dimensions. Nanoporous metals have attracted attention both for their intrinsic scientific interest [1, 2] and due to their potential use as actuators [3], biosensors [4], fuel cell electrodes [5], and in bone tissue engineering [6]. To realize these promising uses, fundamental understanding of nanoporous metal stability and morphological evolution is necessary. Based on atomistic simulations of model nanoporous gold, we suggest a coarsening mech-

*Corresponding author
Email address: kkolluri@mit.edu (Kedarnath Kolluri)

anism that may explain certain puzzling experimental observations, namely the occurrence of voids enclosed in ligaments and reduction in volume during synthesis of nanoporous gold.

Nanoporous metals are commonly synthesized by dealloying, in which less noble components of an alloy are electrochemically dissolved. For example, nanoporous gold (np-Au) is synthesized by dissolving silver from a silver-rich gold-silver alloy [7]. Other examples include synthesis by dealloying of np-platinum from PtAg alloys [8] or PtSi alloys [9, 10], and np-copper from AlCu alloys [11]. Initial understanding of the formation and coarsening of np-Au was based on on-lattice surface diffusion of gold atoms [12]: as silver atoms are removed, gold atoms diffuse on the surfaces thereby exposed and attach to terraces and hillocks, causing the np-Au to coarsen. Such a model, however, is not sufficient to explain all experimental observations on np-Au formation. An on-lattice model assumes that the number of atomic sites remains constant and, therefore, predicts that the volume of the np-Au remains fixed during dealloying whereas the volume of samples reduces by as much as 30% in some synthesis procedures [1, 13]. A coarsening model based only on surface diffusion would predict that enclosed voids would not form whereas ligaments in some np-Au samples were found to contain voids [14]. Furthermore, surface diffusion-dominated coarsening would predict that regions with large positive or negative curvature such as ligament pinch-off regions are quickly smoothed out. Remnants of ligament pinch-off, however, have been observed in experiments [34].

Because several np-Au samples were found to contain lattice defects such as stacking faults, twins, and dislocations [1, 13, 15, 16], it has been suggested that localized plastic deformation may cause volume reduction during dealloying. Nonetheless, a detailed picture of how plastic deformation—a volume conserving process—may lead to volume reduction and the formation of internal voids is lacking. Based on atomic-scale simulations of model np-Au, we suggest a mechanism by which plastic deformation may lead to coarsening of nanoporous metals. The mechanism we suggest could also explain other phenomena observed during dealloying in experiments, namely densification of np-Au and formation of

enclosed voids.

The formation and coarsening mechanisms of np-Au are difficult to determine by experiments alone since the spatio-temporal resolution required to directly observe the relevant processes often exceeds current capabilities. Unfortunately, a realistic representation of dealloying chemistry and time scales is also beyond the current capabilities of atomic-scale simulations. We therefore investigate the morphological evolution of a model np-Au structure that, while it does not directly correspond to the experimental dealloying process, shares some important structural properties with real np-Au. Using atomistic simulations, we find that this model np-Au coarsens by restructuring its open-cell network by collapse of neighboring ligaments onto each other. The ligament collapse is made possible by concurrent localized plasticity at ligaments and nodes. The restructuring of the np-Au network causes volume reduction and coarsening and on occasion leads to formation of voids completely enclosed in ligaments. Such a coarsening mechanism may be operative in the early stages of formation of real np-Au and may explain some experimental observations that a surface diffusion-dominated mechanism alone cannot. In addition, the proposed mechanism predicts a critical ligament radius below which such plasticity-mediated coarsening would occur spontaneously, setting a lower limit to the ligament dimensions of nanofoams.

2. Model and methods

In our atomistic simulations, interatomic interactions are modeled using an embedded atom method (EAM) potential for gold [17] (A review of EAM potential methodology can be found in reference [18] and a recent review of interatomic potentials for metals can be found in reference [19]). This EAM potential was fit to the equilibrium lattice constant, sublimation energy, bulk modulus, elastic constants, and vacancy formation energy of fcc Au [17]. It also predicts well other properties such as the melting point and that Au is most stable in the face-centered cubic structure [17, 20]. This EAM potential also agrees well with

the universal equation-of-state by Rose and co-workers [21] and the experimentally determined radial distribution function of liquid gold [20]. Additionally, the EAM potential used in this study predicts correctly the trends in surface energy for different surface orientations [17, 20], which is crucial in studies of nanoporous metals since surfaces make up for a large fraction of the material.

The stable stacking fault energy of 6 mJ/m^2 predicted by this EAM potential is much lower than the stacking fault energy of 32.5 mJ/m^2 for real gold [20]. Nonetheless, the unstable stacking fault energy of 102.9 mJ/m^2, which governs the barriers that must be overcome for glide dislocation nucleation, predicted by this EAM potential is nearly identical to 101.8 mJ/m^2 predicted by a more-recent EAM potential [22]. Therefore, we expect that the lengths of stacking-fault ribbons in simulated np-Au would be longer than in real np-Au, but the qualitative nature of dislocation nucleation would not change.

To create a model nanoporous structure, $N = 500000$ atoms were placed in a simulation cell under periodic boundary conditions. The size of the simulation cell was chosen to obtain an np-Au of desired density. For example, in order to create a nanoporous gold of relative density ($\rho_{rel} = \frac{\rho}{\rho_{Au}}$) 0.2, the simulation cell in each dimension was chosen to be $a_{Au} \times \sqrt[3]{\frac{N}{4*\rho_{rel}}} = 34.883$ nm where $a_{Au} = 0.408$ nm is the equilibrium lattice parameter of pure gold at 0 K. Initially, an expanded fcc structure with lattice parameter equal to $\frac{a_{Au}}{\sqrt[3]{\rho_{rel}}}$ was filled with atoms after which each atom was moved randomly with displacement in each of the three directions chosen by uniform sampling in the range (−1 nm,1 nm). The system was subsequently relaxed at constant volume using conjugate gradient potential energy minimization (PEM) [23] for 150000 iterations.

The initially random distribution of atoms spontaneously aggregates into a foam-like structure, similar to those observed in previous simulations of processes ranging from homogeneous liquid-vapor nucleation in fluids [24, 25, 26] to macroscale galaxy redistribution in the universe [27]. In addition to the aggregate foam-like structure, the simulation cell also contains free-standing clusters of atoms. These clusters form because the distance between their surfaces and the interconnected foam exceeds the range of the EAM potential used in this

study and because there are no long-range (e.g. electrostatic) or body (e.g. gravitational) forces in our model. Most free-standing clusters contain 1 to 200 atoms. For example, foam-like structure made with $\rho_{rel} = 0.2$ contains 1543 clusters with 2 clusters containing about 1300 atoms, 12 clusters containing between 500 and 1000 atoms, 30 clusters containing between 200 and 500 atoms, and the rest containing less than 200 atoms. A total of 9% of the atoms are contained in these free-standing clusters for a foam-like structure for $\rho_{rel} = 0.2$.

The resulting foam-like structure is a solid. The first, third and fourth peaks in the pair correlation function, while broader than that for a deformed single crystal, were clearly discernable and centered around the values expected for fcc Au. The second neighbor peak was reduced due to the presence of large percentage of atoms at free surfaces. This structure was annealed at 300 K (maintained constant by velocity rescaling [23]) for ~ 0.8 ns using molecular dynamics (MD) simulations [23] with a time step of 0.8 femtoseconds, during which the np-Au coarsens. As a consequence of coarsening, most free-standing clusters of atoms become attached to the nanoporous Au. The remaining few free-standing clusters are removed and the potential energy of the resulting structure is minimized again. In order to confirm that the presence of clusters has negligible effect on coarsening, a representative nanofoam resulting after removing the few remaining clusters was annealed at 300 K for another ~ 1 ns. The nanofoam continued to coarsen with no appreciable change in coarsening rate [Fig. 2(a)], confirming that the free-standing clusters have negligible effect on coarsening. Three different final relative densities, $\rho_{rel} = \frac{\rho}{\rho_{Au}} \in \{0.19, 0.3, 0.42\}$, were considered in this investigation. Annealing was performed at both constant volume and at constant zero pressure.

Diffusion, a thermally activated process, is not expected to occur during the simulations described above. No thermally activated phenomena can occur during potential energy minimization. Molecular-dynamics simulations performed at 300 K would require a run of several nanoseconds for a single atom jump to occur, given migration barriers typically found in metals [17]. Therefore, we expect negligible surface diffusion in the timescale of our study (about 1

nanosecond). Consequently, the phenomena observed in our simulations are caused by processes other than diffusion.

Simulations were performed using LAMMPS [28]. The ligament and pore radii of the nanoporous structures were determined using pore-size distribution functions [29]. Figure 1 shows a visualization of a typical np-Au structure obtained using this procedure. Structural features such as atoms in face-centered cubic (fcc) environments, stacking faults, twins, and dislocation cores were characterized using common neighbor analysis [30]. Prevailing crystallographic orientations along free surfaces were determined by analyzing surface radial distribution functions [23]. AtomEye [31] and VisIt [32] were used for visualization.

3. Structural features of model np-Au

The model np-Au, like that shown in Fig. 1, is always open cell with interconnected ligaments. As most real np-Au, the model structures are crystalline and face-centered cubic with the lattice parameter corresponding to that of fcc gold [1, 7, 15, 33] and the ligament surface normals of model np-Au are predominantly in the crystallographic $\langle 111 \rangle$ direction [34]. Like some real np-Au [33], our model np-Au systems are polycrystalline with grain sizes comparable to ligament dimensions. The model np-Au contains lattice defects such as dislocations, stacking faults, and twin boundaries; such defects have been observed in real np-Au [1, 13, 15, 16]. Like some real np-Au [14], three or four ligaments typically meet each other at nodes in the model np-Au we obtained (determined by visual inspection; see Fig. 1). The local curvatures of each ligament in the model np-Au vary, with curvatures changing from positive to negative, sometimes more than once along a single ligament (determined by visual inspection; see Fig. 1). Similar variation in mean curvature was observed in real np-Au as well [14, 34, 35].

The average ligament and pore sizes in model np-Au structures are much smaller than those found in experiments. The average ligament radii in model np-Au are in the range $1.5 - 2.1$ nm while the average pore radii are in the range $6.7 - 4.8$ nm. By contrast, ligament radii of experimental ones ranged

between 5 and 50 nm for the same range of relative densities [14, 15, 16, 35, 36, 37]. A possible consequence of this difference is that our model may be more representative of np-Au in the initial stages of dealloying where ligament radii may be much smaller than those finally measured [14, 15, 16, 35, 36, 37]. Despite this discrepancy, just as some experimentally synthesized np-Au structures [14], the ligament and pore radii of model np-Au scale with their relative densities in the same manner as conventional open cell foams do [38]. We found that the relative densities of our model np-Au are related to ligament and pore radii by the vertex-corrected scaling expression given by Eqn. 1 [38] where r_l and r_p are ligament and pore radii, respectively, with $C_2 = 4.38 \pm 0.23$ and $D_2 = 4.93 \pm 0.58$.

$$\rho_{\text{rel}} = C_2 \left(\frac{r_l}{r_p} \right)^2 \left[1 - D_2 \left(\frac{r_l}{r_p} \right) \right] \tag{1}$$

Model np-Au increased in density when annealed at zero pressure. An increase of $\sim$ 33% in density was observed for np-Au that were initially 19% dense and an increase of $\sim$ 25% in density was observed for np-Au that were initially 30% dense. Furthermore, enclosed voids are observed in model np-Au with $\rho_{rel} \in \{0.3, 0.42\}$ annealed at constant volume. The average radius of the enclosed voids ranged from 0.65 nm to 1.35 nm. For comparison, voids with radii ranging from 0.5 nm to 2.5 nm have been observed in real np-Au with 16 nm radius ligaments [14].

All of the structural and topological features present in model np-Au have been observed in differently synthesized real nanoporous materials, as described above. It appears that the main discrepancy between the model np-Au and real nanoporous materials is that no one real nanoporous material exhibits all of the structural features of the model. How this discrepancy may reflect on differences in properties requires further investigation, but we believe that it would not alter qualitatively the results presented in this manuscript.

4. Coarsening during annealing of model np-Au

Model np-Au samples coarsen during annealing at 300 K. Figure 2(a) shows the evolution of the average ligament size and number of surface atoms during

annealing of a 19% dense np-Au at 300 K and constant volume. Atoms in free-standing clusters are counted neither when computing the number of surface atoms nor in determining the ligament radii shown in Fig. 2(a). The vertical line marks the point where remaining free-standing clusters were removed. Subsequent annealing of the nanofoam shows that the clusters have negligible effect on nanofoam coarsening. As annealing proceeds, surface atoms reduce in number while simultaneously the average ligament radius increases. We found that the np-Au coarsens by collapse onto each other of neighboring ligaments resulting in a net reduction of free surface area and formation of thicker ligaments. Two representative examples of ligament collapse during annealing of a 19% dense np-Au at 300K and constant volume are shown in Fig. 3(a)-(c) and Fig. 3(d)-(f), where each panel is a sequence of snapshots leading to one collapse event. In both cases, the collapse is aided by plastic deformation at nearby nodes. In Fig. 3(a)-3(c), dislocation glide enables shearing initially at the bases of adjacent ligaments connecting to the same nodes and then in the ligaments themselves, allowing their "displacive" movement toward each other and eventual collapse into one ligament.

In Fig. 3(d)-3(f), the indicated ligament pinches off, followed by collapse of other nearby ligaments onto each other. The ligament pinch off occurs by dislocation glide across the ligament cross-section. As in the example in Fig. 3(a)-3(c), here also plastic deformation enables network reconstruction. Although the ligament pinchoff creates additional free surface area, the associated energy increase is more than compensated by the decrease in energy arising from the removal of free surfaces due to accompanying collapse of neighboring ligaments onto each other.

While there appear to be two regimes with different coarsening rates in Fig. 2(a), they differ primarily in the number of collapse events. Initially, the ligaments are sufficiently thin and close that the collapse rate, and therefore also the coarsening rate, is high. As the average ligament and pore sizes increase, the average distance between ligaments also increases. The increased ligament size implies that a higher plastic work rate is required to maintain a given coarsening

rate. Increased pore size also implies that greater plastic work is necessary for equal number of collapse events. Therefore, the coarsening rate reduces as the ligament radius increases. Since the coarsening rate is likely dependent on both ligament and pore radius and because the ligament and pore radius can be related to each other by the relative density as in Eqn. 1, the rate of coarsening by network restructuring is likely dependent on the relative density.

No appreciable migration of surface atoms by thermally activated diffusion was observed during the annealing process. In model np-Au, atoms that are at the free surface at the end of the annealing process moved on average by about 0.45 nm from their initial neighbors. For coarsening to occur by surface diffusion, however, the average surface atom migration distance would have to have been of the same order as the ligament length or the pore radius, which is in the range 6.7−4.8 nm in our simulations. The observed atomic motion is likely due to surfaces relaxing to their lowest energy orientations. It may aid in the onset of local plastic deformation and thereby contribute to coarsening indirectly [39].

5. Coarsening during deformation of model np-Au

Since localized plastic deformation is required for coarsening by the mechanism described above, it may be expected that application of an external load may also promote coarsening. To test this hypothesis, volume-conserving uniaxial compression ($\epsilon_{zz} < 0$, $\epsilon_{yy} = \epsilon_{xx} > 0$) was performed at zero temperature on np-Au samples that were annealed for ~ 0.8 ns, with small remaining clusters removed, and the resulting structure relaxed by potential energy minimization. Model np-Au were compressed along the z direction at strain increments of 0.99% while the x and y cell dimensions were extended such that the total volume of the simulation cell remained constant. The strain applied to the model np-Au was therefore purely deviatoric. After each strain increment the model was relaxed at zero temperature by PEM until the maximum force on any atom was less than 5 pN. All the samples were found to coarsen during the deformation [Fig. 2(b)]. At sufficiently low applied tensile equivalent strains ϵ_{dev}, local

plastic deformation occurs but does not cause ligament pinchoff or collapse. Upon further deformation, however, ligament pinchoff and associated network reconstruction do occur and cause coarsening. Just as during annealing, where events like those shown in Fig. 3(a)-3(c) and Fig. 3(d)-3(f) take place, pinchoff and collapse of neighboring ligaments onto each other are also observed upon deformation, as illustrated in Fig. 3(g)-3(i).

In addition, model np-Au at all densities investigated exhibited an elastic-perfect plastic stress-strain response [Fig. 4(a)] reminiscent of the behavior of conventional metallic foams [38] and qualitatively similar to that found in experiments on np-Au [36]. A critical tensile yield strength for gold of $\sigma_s = 3.864$ GPa may be backed out by fitting the average flow stress [Fig. 4(b)], which is also the average yield stress in the case of materials exhibiting elastic-perfect plastic response, in the applied strain range $0.1 \leq \epsilon_{dev} \leq 0.3$ with the Gibson-Ashby scaling equation for plastically collapsing foams. The Gibson-Ashby scaling equation, Eqn. 2, [38] relates relative foam density (ρ_{rel}), average plastic yield stress of the foam (σ), and the yield strength of the foam material (σ_s) where $C = 0.3$ [38].

$$\frac{\sigma}{\sigma_s} = C\rho_{rel}^{3/2} \tag{2}$$

Assuming that the ligament axes are on-average oriented along $\langle 110 \rangle$ directions (the Schmid factor for slip along $\{111\}$ $\langle 112 \rangle$ is then ~ 0.47), a critical resolved shear stress for deformation of 1.8 GPa is obtained and is in good agreement with the critical shear stress of model single crystal gold used in our simulations ($\sigma_s^{ideal} = 1.92$ GPa for the same slip system). The critical shear stress for model single crystal gold was calculated by a simple shear deformation on a $\{111\}$ plane along a $\langle 112 \rangle$ direction of a supercell single crystal gold using the same EAM potential [17] used to simulate model np-Au. Some experimentally measured yield stresses in np-Au were in good agreement with the Gibson-Ashby scaling expression when modified to account for ligament size dependence of yield stress [40]. Modification of the Gibson-Ashby scaling relation to account for size effects is not required in our study as the ligament radii in

the model np-Au considered do not vary over a wide enough range.

6. Enclosed voids in model np-Au

A coarsening mechanism involving reconstruction of the nanoporous network may elucidate experimental observations that cannot be explained by coarsening through surface diffusion alone. For example, internal voids may form when collapsing ligaments are not perfectly contiguous. Figure 5 shows sections of a 30% dense np-Au as it coarsens during annealing at constant volume. The np-Au in the top panel is sectioned to make visible an internal void. In Fig. 5(a)-(d), which shows successive stages of coarsening, surface atoms on both ligaments and internal voids are colored black while the lighter atoms are inside ligaments and nodes. The bottom panel, Fig. 5(e)-5(h), shows a three dimensional view of the section marked in Fig. 5(a). In the bottom panel free surfaces are colored in transparent red while interiors of ligaments and nodes are colored transparent green. In Fig. 5(e), six ligaments that eventually collapse to form an internal void are marked. As they collapse, some regions along these ligaments are closer to each other than others, as indicated by the arrows in Fig. 5(f). If the collapsing surfaces completely enclose other surfaces that are further apart, voids may form. Such a scenario is played out in Fig. 5(f)-(h) where the regions marked with arrows collapse sequentially to leave an internal void, marked in Fig. 5(h).

The mechanism described above contrasts with a recently proposed surface-diffusion-based alternative explanation for formation of enclosed voids [44]. In this alternative explanation, based on kinetic Monte Carlo simulations performed on simulated dealloyed nanoparticles, it has been suggested that surface diffusion in nanoporous structures leads to pulling away of material from saddle-point curvature ligaments, with the geometric effect of reducing the topological genus. Such pulling away of material leads eventually to ligament pinch-off associated with Rayleigh instabilities, and this also leads to bubble formation. In our view, the mechanism proposed in [44] offers a competing, though not contradictory, explanation to that presented here.

7. Critical ligament radius for spontaneous coarsening

Our simulations show that coarsening in some nanoporous metals may arise from network restructuring accompanied by localized plasticity. For nanoporous structures with sufficiently small ligament radii, the rate of surface energy reduction during coarsening may be greater than the rate of plastic work. If so, coarsening by this mechanism may occur spontaneously without thermal activation until ligament radii reach a critical value. For ligament radii beyond this value, the rate of plastic work exceeds the rate of surface energy reduction. To develop an estimate of this critical radius, we consider a nanoporous material consisting of ligaments with average ligament radius R and average ligament length L, which is proportional to the pore radius. Suppose that collapse of a fraction p_1 of the ligaments leads to an increase dR in the average ligament radius and corresponding decrease in surface area. As shown in Fig. 3, some of these events are accompanied by pinch-off of nearby ligaments, which increases the free surface area. To account for this, we assume that a fraction p_2 of the ligaments that pinch off do not collapse. We also assume that the density remains constant during coarsening, though this is not strictly necessary.

The incremental decrease in the per ligament surface energy due to the reduction in the surface area is then given by

$$dE_{surface} = [C_0 p_1 2\pi\gamma L - p_2 4\pi\gamma R]dR \tag{3}$$

where the first term corresponds to the surface area removed by the collapse of ligaments and the second is the additional surface area created at pinched-off ligaments. C_0 is a measure of the extent of collapse of ligaments onto each other and reaches its maximum value $C_{0_{max}} = 2 - \sqrt[3]{2} = 0.74$ at constant np-Au density and when all ligaments collapse onto their neighboring ones without forming any enclosed voids. At constant density, L and R are related by Eqn. 1. For simplicity, we retain only the leading order term $R \approx L\ C_2^{'}\sqrt{\rho}_{rel}$ where $C_2^{'} = C_2^{-\frac{1}{2}}$ is obtained by fitting data from our simulations. The incremental

decrease in surface energy per ligament can then be rewritten as

$$dE_{surface} = 2\pi p_1 \frac{K_1}{C_2' \sqrt{\rho}_{rel}} \gamma R dR \text{ where } K_1 \approx (C_0 - 2\frac{p_2}{p_1} C_2' \sqrt{\rho}_{rel}). \tag{4}$$

.

The plastic work required for ligament collapse may be estimated as follows. Since the localized plasticity is caused by dislocation glide, the average plastic work for each dislocation is the amount of work required to move a dislocation across a ligament. The glide of one dislocation causes a displacement equal to the Burgers vector b of the dislocation. Since the average displacement required for ligament collapse is proportional to the pore radius, the number of dislocations that must glide through a ligament on average is $\frac{1}{K_0}\frac{L}{b}$ where L is the distance a ligament must be displaced to collapse into one of its neighbors and K_0 is a constant parameter of order one. Therefore, the associated increment of plastic work per ligament is given by

$$dW_{plastic} = p_1[\tau b(2\pi R dR)](\frac{1}{K_0}\frac{L}{b}). \tag{5}$$

Coarsening by the postulated mechanism will occur spontaneously if $\frac{dW_{plastic}}{dR} < \frac{dE_{surface}}{dR}$. To compute the critical ligament radius beyond which the postulated mechanism does not occur spontaneously, we set the two terms equal and get

$$R^* = K\frac{\gamma}{\tau} \text{ where } K = K_0(C_0 - 2\frac{p_2}{p_1} C_2' \sqrt{\rho}_{rel}) \tag{6}$$

The critical radius R^* below which coarsening by network restructuring occurs spontaneously decreases with plastic flow resistance, increases with surface energy, and depends on the nanoporous network topology and the statistics of ligament collapse and pinch-off events through the constant K. Furthermore, Eqn. 6 predicts a network topology-dependent critical pinchoff fraction beyond which the surface area increase is too large to be compensated by ligament collapse. Thus, it may be possible to design nanoporous networks that are less susceptible to coarsening by the proposed mechanism, even though ligament collapse may still occur at isolated locations during annealing and ligament collapse may lead to coarsening when external loading is applied.

For a numerical estimate of the critical radius, we assume that collapsed ligaments greatly exceed those that pinch off ($K = K_0 C_0$) and that all ligaments fully collapse ($C_0 = 0.74$). We assume the flow resistance to be $\tau = 800$ MPa. This is the lowest flow stresses for Au nanopillars observed in compression of 250 nm radius gold cylinders [41], although other studies suggest that the relevant flow resistance could be as high as 2.5 GPa [42]. We also assume that on average the ligaments must be displaced by half the pore radius to collapse onto an adjacent ligament, i.e., $K_0 = 2$. For $\gamma_{\{111\}_{Au}} = 1.25$ J/m^2 [43], we get $R^*_{Au} \approx 3.2$ nm. For the range of permissible values for τ and K_0, the critical radius R^*_{Au} ranges between 1 nm and 10 nm. This range of predicted critical radii for np-Au lies below the average ligament radii reported in all experiments on np-Au of which we are aware [14, 15, 16, 35, 36, 37, 40], suggesting that coarsening by the mechanism described here may be operating very early in the dealloying and coarsening process.

8. Conclusions

Atomistic simulations reveal that coarsening of model np-Au may occur by network restructuring caused by neighboring ligaments collapsing onto each other. This process is accompanied by localized plasticity at nodes and within the ligaments themselves. An expression is developed for a critical radius below which this mechanism may operate spontaneously, suggesting that synthesis of nanoporous materials with ligament radii below of a few nanometers might not be possible unless their surface energy, flow resistance, and network topology are tailored to increase the plastic work rate during coarsening beyond the rate of associated surface energy reduction. Although direct experimental verification of whether coarsening occurs by collapse of adjacent ligaments is still not currently possible, presently available experimental data provide indirect support to the mechanism we suggest: ligaments with high curvature corresponding to pinch-off events have been observed in nanoporous samples, even when no external load is applied [34]; enclosed voids form in nanoporous metals [14]; and np-Au is known to densify during dealloying, annealing [1], and deformation

[33]. Continued development of multi length- and time-scale characterization methods eventually enable validation of the coarsening mechanism proposed here by direct observation [45].

9. Acknowledgments

This work was partially supported by a user grant from the Center for Integrated Nanotechnologies (CINT) at Los Alamos National Laboratory (LANL). We thank A. Misra, A. Antoniou, A. S. Argon, W. C. Carter, and L. J. Gibson for many useful discussions and helpful insights as well as K. J. Van Vliet and M. Kabir for help with computing resources during the initial stages of this work. K. K. thanks R. E. Baumer for help with visualization tools.

References

[1] S. Parida, D. Kramer, C. A. Volkert, H. Rösner, J. Erlebacher, J. Weissmüller, Volume change during the formation of nanoporous gold by dealloying, Phys. Rev. Lett. 97 (3) (2006) 035504.

[2] H. Li, A. Misra, A dramatic increase in the strength of a nanoporous Pt-Ni alloy induced by annealing, Scripta Materialia 63 (12) (2010) 1169 – 1172.

[3] J. Biener, A. Wittstock, L. A. Zepeda-Ruiz, M. M. Biener, V. Zielasek, D. Kramer, R. N. Viswanath, J. Weissmueller, M. Baeumer, A. V. Hamza, Surface-chemistry-driven actuation in nanoporous gold, Nature Materials 8 (1) (2009) 47–51.

[4] K. Hu, D. Lan, X. Li, S. Zhang, Electrochemical DNA biosensor based on nanoporous gold electrode and multifunctional encoded DNA−Au bio bar codes, Analytical Chemistry 80 (23) (2008) 9124–9130.

[5] J. Snyder, T. Fujita, M. . W. Chen, J. Erlebacher, Oxygen reduction in nanoporous metal-ionic liquid composite electrocatalysts., Nature Materials 9 (11) (2010) 904–907.

[6] E. E. L. Swan, K. C. Popat, T. A. Desai, Peptide-immobilized nanoporous alumina membranes for enhanced osteoblast adhesion, Biomaterials 26 (14) (2005) 1969 – 1976.

[7] J. Erlebacher, M. Aziz, A. Karma, N. Dimitrov, K. Sieradzki, Evolution of nanoporosity in dealloying, Nature 410 (6827) (2001) 450–453.

[8] H.-J. Jin, D. Kramer, Y. Ivanisenko, J. Weissmüller, Macroscopically strong nanoporous Pt prepared by dealloying, Advanced Engineering Materials 9 (10) (2007) 849–854.

[9] A. Antoniou, D. Bhattacharrya, J. K. Baldwin, P. Goodwin, M. Nastasi, S. T. Picraux, A. Misra, Controlled nanoporous pt morphologies by varying deposition parameters, Applied Physics Letters 95 (7) (2009) 073116.

[10] J. C. Thorp, K. Sieradzki, L. Tang, P. A. Crozier, A. Misra, M. Nastasi, D. Mitlin, S. T. Picraux, Formation of nanoporous noble metal thin films by electrochemical dealloying of Pt_xSi_{1-x}, Applied Physics Letters 88 (3) (2006) 033110.

[11] Z. Qi, C. Zhao, X. Wang, J. Lin, W. Shao, Z. Zhang, X. Bian, Formation and characterization of monolithic nanoporous copper by chemical dealloying of Al−Cu alloys, The Journal of Physical Chemistry C 113 (16) (2009) 6694–6698.

[12] J. Erlebacher, An atomistic description of dealloying, Journal of The Electrochemical Society 151 (10) (2004) C614–C626.

[13] H.-J. Jin, L. Kurmanaeva, J. Schmauch, H. Rösner, Y. Ivanisenko, J. Weissmüller, Deforming nanoporous metal: Role of lattice coherency, Acta Materialia 57 (9) (2009) 2665 – 2672.

[14] H. Roesner, S. Parida, D. Kramer, C. A. Volkert, J. Weissmueller, Reconstructing a nanoporous metal in three dimensions: An electron tomography study of dealloyed gold leaf, Advanced Engineering Materials 9 (7) (2007) 535–541.

[15] Y. Sun, J. Ye, Z. Shan, A. Minor, T. Balk, The mechanical behavior of nanoporous gold thin films, JOM Journal of the Minerals, Metals and Materials Society 59 (2007) 54–58.

[16] S. V. Petegem, S. Brandstetter, R. Maass, A. M. Hodge, B. S. El-Dasher, J. Biener, B. Schmitt, C. Borca, H. V. Swygenhoven, On the microstructure of nanoporous gold: An x-ray diffraction study, Nano Letters 9 (3) (2009) 1158–1163.

[17] S. M. Foiles, M. I. Baskes, M. S. Daw, Embedded-atom-method functions for the fcc metals Cu, Ag, Au, Ni, Pd, Pt, and their alloys, Physical Review B 33 (12) (1986) 7983–7991.

[18] M. S. Daw, S. M. Foiles, M. I. Baskes, Materials science reports 9 (1993) 251–310.

[19] J. H. Li, X. D. Dai, S. H. Liang, K. P. Tai, Y. Kong, B. X. Liu, Physics reports 455 (2008), 1–134.

[20] G. Grochola, S. P. Russo, I. K. Snook, On fitting a gold embedded atom method potential using the force matching method, The Journal of Chemical Physics 123 (20) (2005) 204719.

[21] J. H. Rose, J. R. Smith, F. Guinea,J. Ferrante, Universal features of the equation of state of metals, Physical Review B 29 (6) (1984) 2963–2969.

[22] H. W. Sheng, M. J. Kramer, A. Cadien, T. Fujita, M. W. Chen, Highly optimized embedded-atom-method potentials for fourteen fcc metals, Physical Review B 83 (13) (2011) 134118

[23] A. M. Allen, D. J. Tildesley, Computer Simulation of Liquids, Oxford University Press, Oxford, 1990.

[24] F. F. Abraham, D. E. Schreiber, M. R. Mruzik, G. M. Pound, Phase separation in fluid systems by spinodal decomposition: A molecular-dynamics simulation, Phys. Rev. Lett. 36 (5) (1976) 261–264.

[25] R. Yamamoto, K. Nakanishi, Computer simulation of vapor-liquid phase separation in two- and three-dimensional fluids: Growth law of domain size, Phys. Rev. B 49 (21) (1994) 14958–14966.

[26] V. K. Shen, P. G. Debenedetti, A computational study of homogeneous liquid–vapor nucleation in the lennard-jones fluid, The Journal of Chemical Physics 111 (8) (1999) 3581–3589.

[27] M. Boylan-Kolchin, V. Springel, S. D. M. White, A. Jenkins, G. Lemson, Resolving cosmic structure formation with the millennium-II simulation, Monthly Notices of the Royal Astronomical Society 398 (3) (2009) 1150–1164.

[28] S. Plimpton, Fast parallel algorithms for short-range molecular-dynamics, J. Comp. Phys. 117 (1) (1995) 1–19.

[29] A. E. Scheidegger, The Physics of Flow Through Porous Media, University of Toronto Press, Toronto, Canada, 1974.

[30] J. D. Honeycutt, H. C. Andersen, Molecular-dynamics study of melting and freezing of small lennard-jones clusters, Journal of Physical Chemistry 91 (19) (1987) 4950–4963.

[31] J. Li, Atomeye: an efficient atomistic configuration viewer, Modelling and Simulation in Materials Science and Engineering 11 (2) (2003) 173–177.

[32] H. Childs, E. S. Brugger, K. S. Bonnell, J. S. Meredith, M. Miller, B. J. Whitlock, N. Max, A contract-based system for large data visualization, in: Proceedings of IEEE Visualization 2005 pp. 190–198.

[33] A. M. Hodge, J. Biener, L. L. Hsiung, Y. M. Wang, A. V. Hamza, J. H. Satcher, Monolithic nanocrystalline Au fabricated by the compaction of nanoscale foam, Journal of Materials Research 20 (3) (2005) 554–557.

[34] Y.-C. K. Chen, Y. S. Chu, J. Yi, I. McNulty, Q. Shen, P. W. Voorhees, D. C. Dunand, Morphological and topological analysis of coarsened nanoporous

gold by x-ray nanotomography, Applied Physics Letters 96 (4) (2010) 043122.

[35] T. Fujita, L.-H. Qian, K. Inoke, J. Erlebacher, M.-W. Chen, Three-dimensional morphology of nanoporous gold, Applied Physics Letters 92 (25) (2008) 251902.

[36] J. Biener, A. M. Hodge, J. R. Hayes, C. A. Volkert, L. A. Zepeda-Ruiz, A. V. Hamza, F. F. Abraham, Size effects on the mechanical behavior of nanoporous Au, Nano Letters 6 (10) (2006) 2379–2382.

[37] T. Fujita, M. W. Chen, Characteristic length scale of bicontinuous nanoporous structure by fast fourier transform, Japanese Journal of Applied Physics 47 (2) (2008) 1161–1163.

[38] L. J. Gibson, M. F. Ashby, Cellular Solids: Structure and Properties, 2nd Edition, Cambridge University Press, Cambridge, United Kingdom, 1997.

[39] D. A. Crowson, D. Farkas, S. G. Corcoran, Geometric relaxation of nanoporous metals: The role of surface relaxation, Scripta Materialia 56 (11) (2007) 919 – 922.

[40] A. Hodge, J. Biener, J. Hayes, P. Bythrow, C. Volkert, A. Hamza, Scaling equation for yield strength of nanoporous open-cell foams, Acta Materialia 55 (4) (2007) 1343 – 1349.

[41] J. R. Greer, W. D. Nix, Nanoscale gold pillars strengthened through dislocation starvation, Physical Review B 73 (24) (2006) 245410.

[42] C. Deng, F. Sansoz, Enabling ultrahigh plastic flow and work hardening in twinned gold nanowires, Nano Letters 9 (4) (2009) 1517–1522.

[43] R. J. Needs, M. Mansfield, Calculations of the surface stress tensor and surface energy of the (111) surfaces of iridium, platinum and gold, Journal of Physics: Condensed Matter 1 (41) (1989) 7555.

[44] J. Erlebacher, Mechanism of Coarsening and Bubble Formation in High-Genus Nanoporous Metals, Physical Review Letters 106 (22) (2011) 225504.

[45] I. M. Robertson, C. A. Schuh, J. S. Vetrano, N. D. Browning, D. P. Field, D. J. Jensen, M. K. Miller, I. Baker, D. C. Dunand, R. Dunin-Borkowski, B. Kabius, T. Kelly, S. Lozano-Perez,A. Misra, G. S. Rohrer, A. D. Rollett, M. L. Taheri, G. B. Thompson, M. Uchic, X-L. Wang, G. Was, Towards an integrated materials characterization toolbox, Journal of Materials Research 26 (2011) 1341–1383.

FIGURE CAPTIONS

FIGURE 1: (Color online) A representative model np-Au with $\rho_{\mathrm{rel}} = 0.19$ formed by relaxation of an initially random distribution of atoms followed by annealing for ∼1 ns. Ligaments, nodes, and pores are indicated. Two representative ligaments in which the curvature changes sign are also shown.

FIGURE 2: Evolution of average ligament radii and percentage of atoms at free surfaces during (a) annealing at 300K of np-Au (19% final density) formed by quenching randomly placed gold atoms and (b) volume-conserving uniaxial compression of 19% dense np-Au annealed for ∼1 ns. The part of the plot to the left of the vertical line in (a) represents annealing of np-Au containing free-standing clusters while the part to the right is for continued annealing of np-Au with all free-standing clusters removed.

FIGURE 3: (Color online) Several examples of collapse of ligaments during (a)-(f) annealing at constant volume and (g)-(i) volume-conserving deformation of 19% dense annealed np-Au. In (a)-(c), the collapse of two neighboring ligaments onto each other is enabled by plastic deformation by dislocation glide, first at the base of the ligaments and then within the ligaments. In (d)-(f), pinchoff of the marked ligament accompanied the collapse of adjacent ligaments onto each other. The horizontal lines in (e) and (f) are guides to the eye showing the direction of ligament collapse. In (g)-(i), two pinched-off ligaments collapse onto one another. In all cases, ligament collapse is made possible by concurrent local plastic deformation at both ligaments and nodes.

FIGURE 4: (Color online) Several examples of collapse of ligaments during (a)-(f) annealing at constant volume and (g)-(i) volume-conserving deformation of 19% dense annealed np-Au. In (a)-(c), the collapse of two neighboring ligaments onto each other is enabled by plastic deformation by dislocation glide, first at the base of the ligaments and then within the ligaments. In (d)-(f),

pinchoff of the marked ligament accompanied the collapse of adjacent ligaments onto each other. The horizontal lines in (e) and (f) are guides to the eye showing the direction of ligament collapse. In (g)-(i), two pinched-off ligaments collapse onto one another. In all cases, ligament collapse is made possible by concurrent local plastic deformation at both ligaments and nodes.

FIGURE 5: (color online) Coarsening during constant volume annealing of a section of 30% dense np-Au. (a)-(d) Black colored atoms are at the surfaces of ligaments or internal voids and other atoms are within the ligaments and nodes. (e)-(h) Three dimensional view of the section marked in (a) where free surfaces are shown in transparent red and ligament interiors are shown transparent green. The collapse of ligaments numbered in (e) leads to the formation of an internal void marked in (h). The corresponding sectioned region of the void is marked in (d).

Fig 1

Click here to download high resolution image

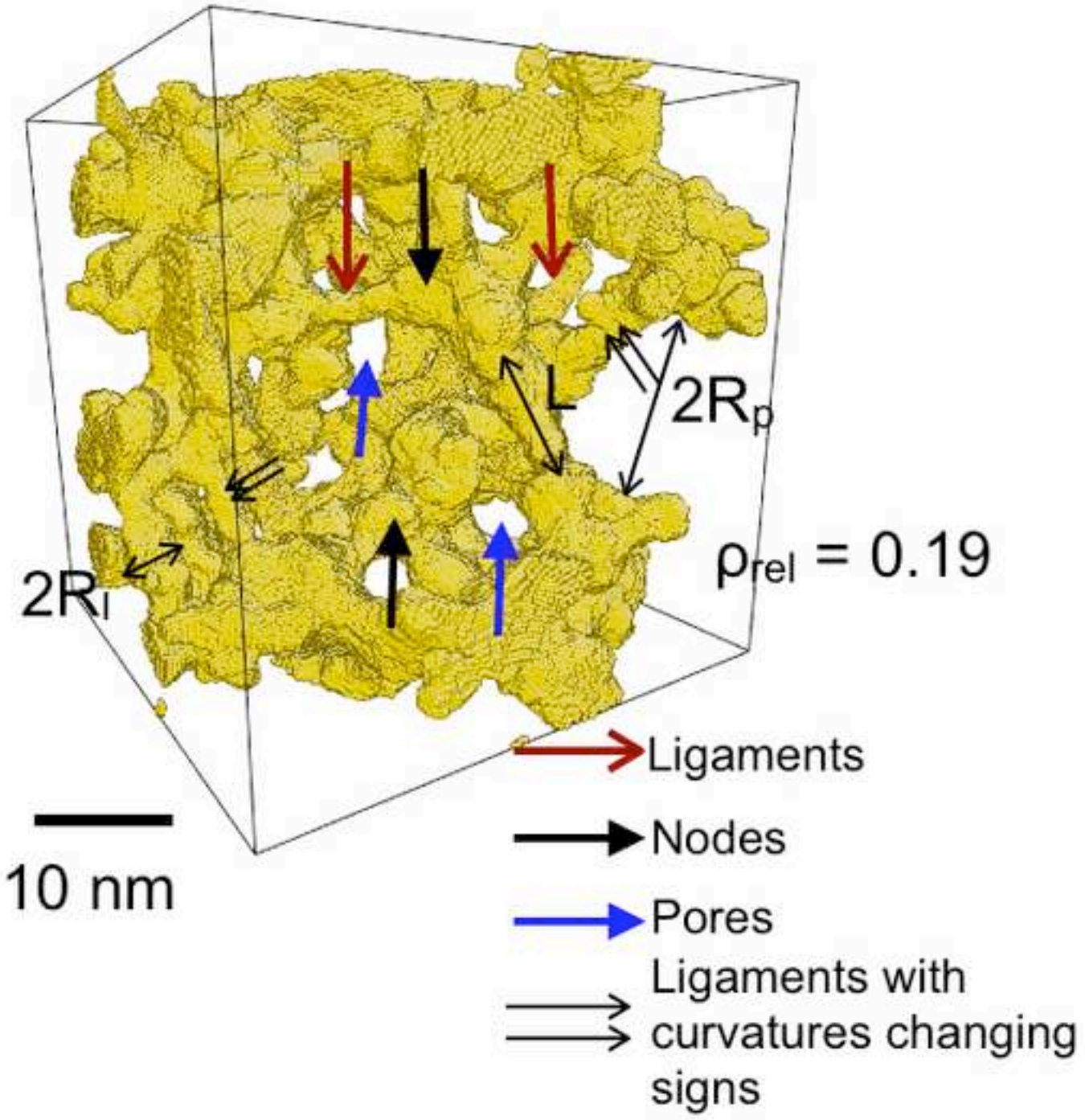

Fig 2

Click here to download high resolution image

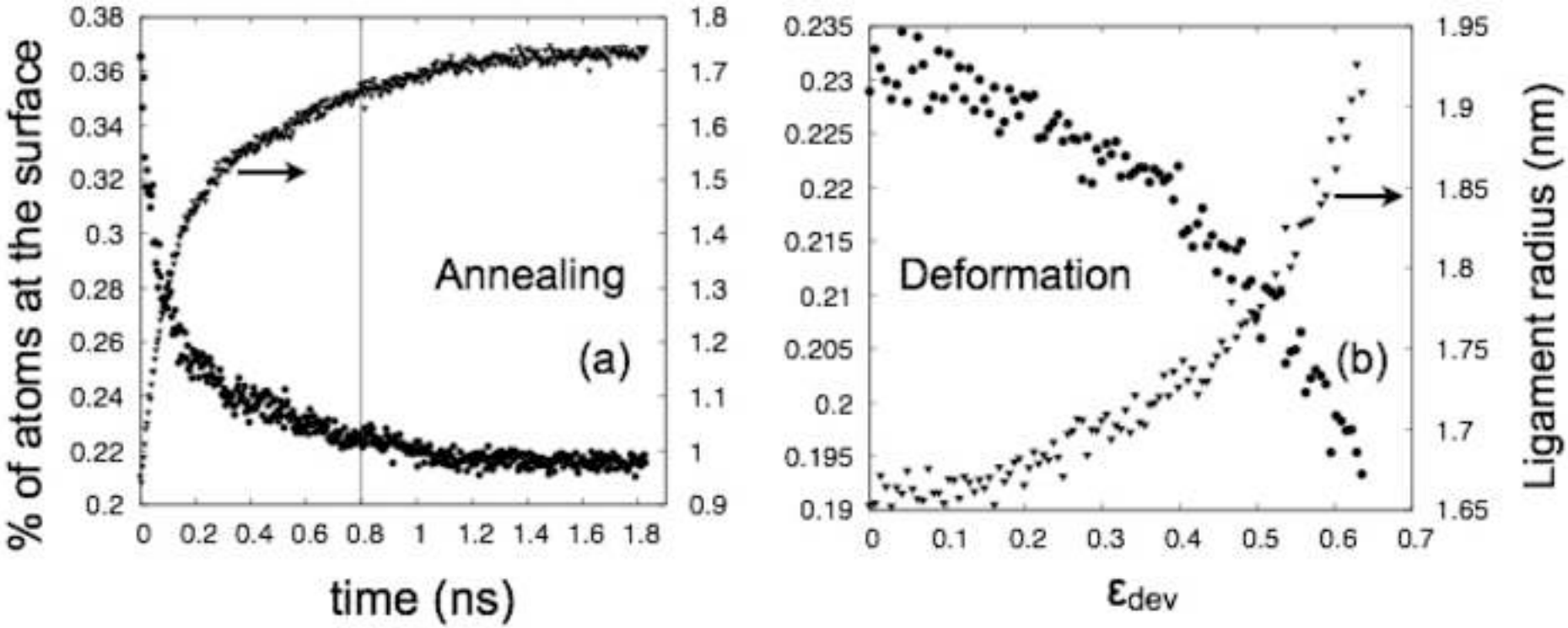

Fig 3

Click here to download high resolution image

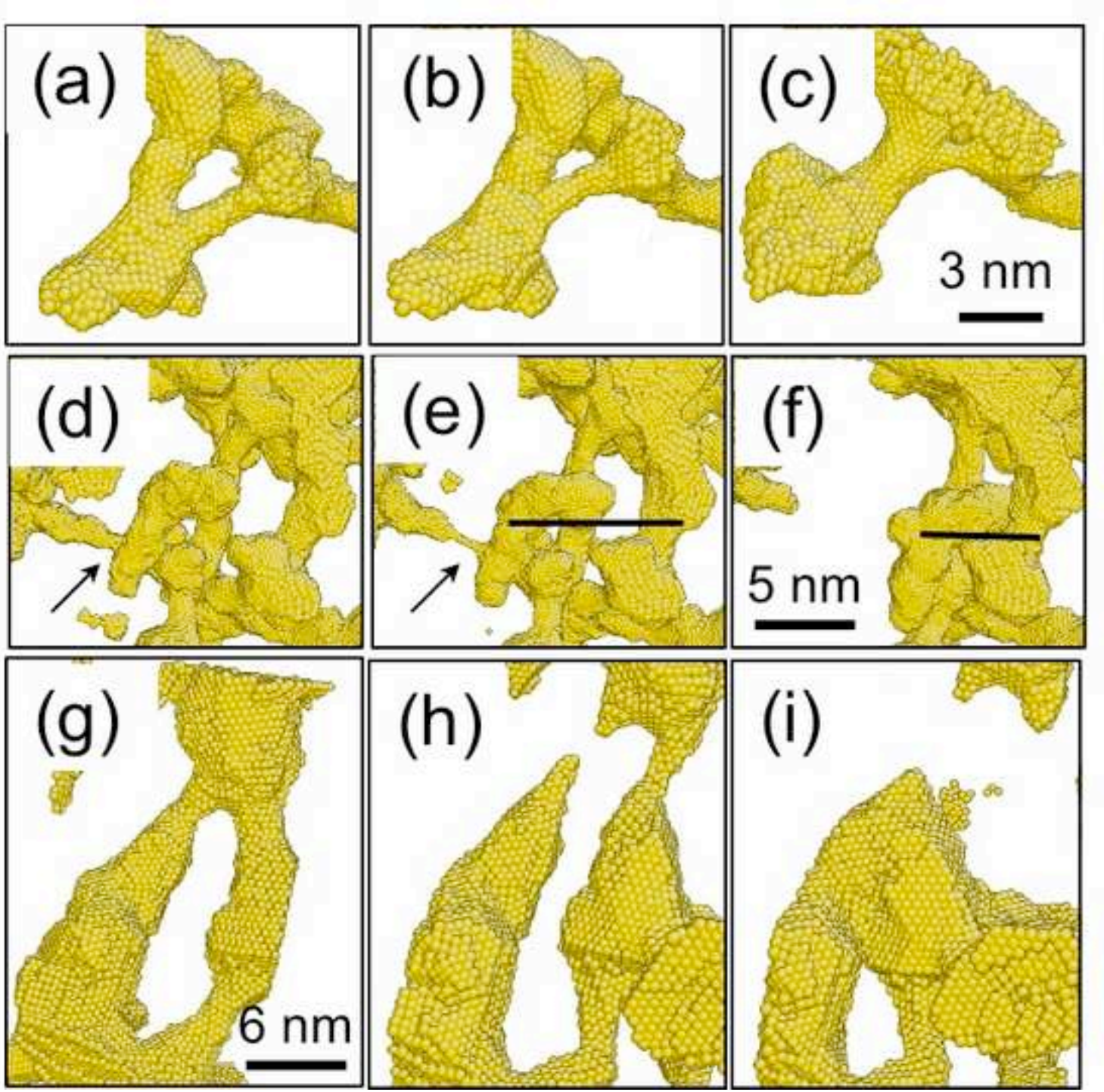

Fig 4

Click here to download high resolution image

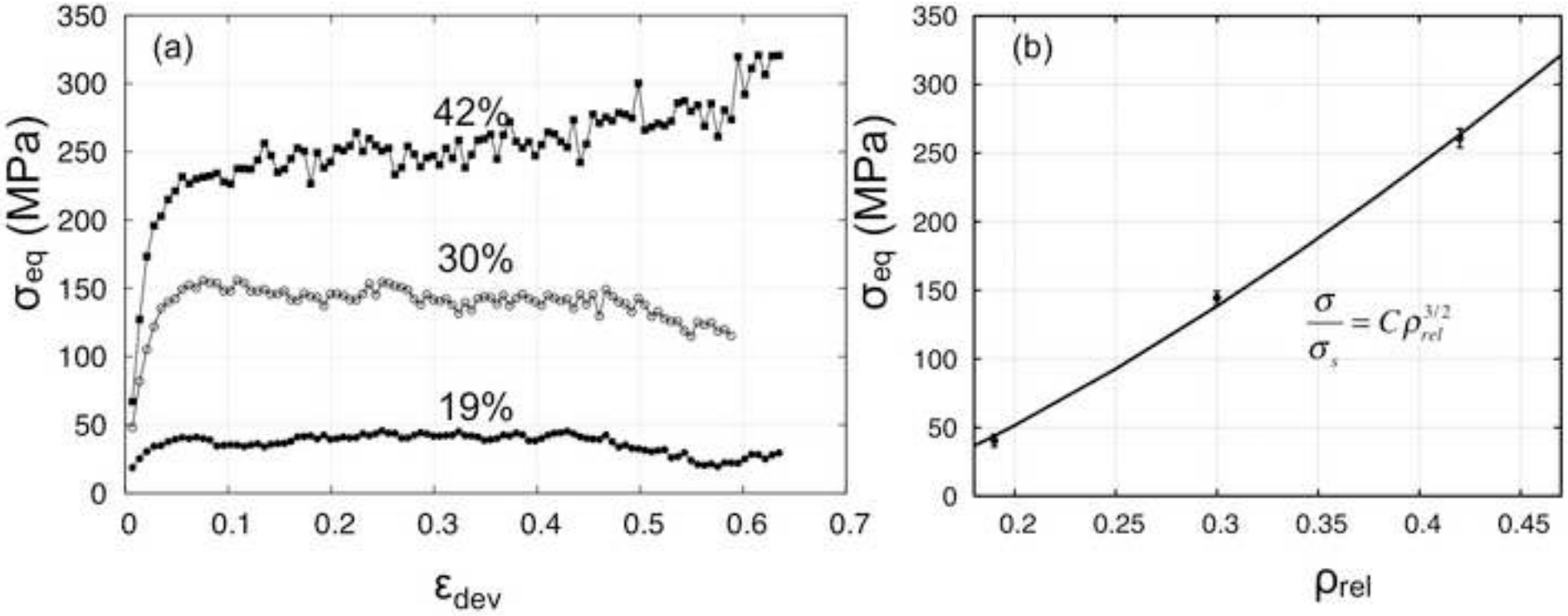

Fig 5

Click here to download high resolution image